Y$_2$O$_3$-MgO Composite Nano-ceramics Prepared from Core-shell Nano-powders

JIANG Hong-tao[1,2], QIN Hai-ming[2,3], FENG Shao-wei[3,4*],
CHEN Hong-bing[1*], JIANG Jun[2,3]

(1. School of Materials Science and Chemical Engineering, Ningbo University, Ningbo 315201, China;
2. Ningbo Institute of Materials Technology and Engineering, Chinese Academy of Sciences, Ningbo 315201, China;
3. University of Chinese Academy of Sciences, Beijing 100049, China;
4. National Engineering Laboratory for Hydrometallurgical Cleaner Production Technology, CAS Key Laboratory of Green Process and Engineering, Institute of Process Engineering, Chinese Academy of Sciences, Beijing 100190, China)
* Corresponding Authors, E-mail：swfeng@ipe.ac.cn; chenhongbing@nbu.edu.cn

Abstract：Y$_2$O$_3$-MgO composite nano-ceramics are regarded as a significant candidate of infrared transparent ceramics on account of excellent optical and mechanical properties. Nevertheless, a huge challenge remains regarding the critical optical scattering and needless absorption in the near- and mid-infrared bands, which hinders its applications in extreme harsh environments. In present work, Y$_2$O$_3$-MgO core-shell structure nano-powders were prepared *via* urea precipitation method before that Y$_2$O$_3$-MgO composite nano-ceramics were prepared under spark plasma sintering. Thermogravimetric and differential scanning calorimetry(TG/DSC), X-ray diffraction and scanning electron microscope were performed to analyze as prepared core-shell structure nano-powders and composite nano-ceramics. The size of Y$_2$O$_3$-MgO core-shell structure nano-powders is about 250 nm, and average grain size of the prepared ceramics is approximately 360 nm. The transmittance is 57% at 6 μm, and the Vickers hardness is 820 HV. The powder synthesis method accomplished in present work offers a novel solution for composite nano-ceramics, which easily regulate particle size and proportion of different components.

Key words：Y$_2$O$_3$-MgO composite nano-ceramics; core-shell structure nano-powder; urea precipitation method; spark plasma sintering

CLC number：O482.31　　　**Document code**：A　　　**DOI**：10.37188/CJL.20210095

核壳纳米粉体制备 Y$_2$O$_3$-MgO 复相陶瓷

江宏涛[1,2]，秦海明[2,3]，冯少尉[3,4*]，陈红兵[1*]，蒋　俊[2,3]

(1. 宁波大学 材料科学与化学工程学院，浙江 宁波　315201；
2. 中国科学院 宁波材料技术与工程研究所，浙江 宁波　315201；3. 中国科学院大学，北京 100049；
4. 中国科学院 过程工程研究所，湿法冶金清洁生产技术国家工程实验室，中科院绿色过程与工程重点实验室，北京　100190)

摘要：由于优异的光学和机械性能，Y$_2$O$_3$-MgO 复相纳米陶瓷被认为是红外透明陶瓷的重要候选材料。尽管

如此,在近红外和中红外波段严重的光散射和不必要的吸收方面仍然存在巨大的挑战,这阻碍了该材料在极端恶劣环境中的应用。在目前的工作中,先通过尿素沉淀法制备了 Y_2O_3-MgO 核壳结构纳米粉体,然后在放电等离子体烧结下制备了 Y_2O_3-MgO 复相纳米陶瓷。通过热重和差示扫描量热法(TG/DSC)、X 射线衍射和扫描电子显微镜分析了核壳结构纳米粉及复相纳米陶瓷。Y_2O_3-MgO 核壳结构纳米粉体的尺寸约为 250 nm,并且制备的陶瓷的平均晶粒尺寸约为 360 nm。透过率在 6 μm 处为 57%,维氏硬度为 820 HV。粉末合成方法为复相纳米陶瓷提供了一种新颖的解决方案,可以轻松调节粒径和不同组分的比例。

关 键 词:Y_2O_3-MgO 复相纳米陶瓷;核壳结构纳米粉体;尿素沉淀法;放电等离子烧结

1 Introduction

In recent years, infrared window materials are brought into focus due to widely used in infrared tracking, identification, search, guidance, navigation, and thermal imaging[1-7]. In order to cope with various application environments, the performance of infrared window materials need to meet the following requirements: infrared transparency, high mechanical strength, high thermal conductivity, and resistance to thermal shock and erosion[5-6]. However, it is not realistic to improve the operational properties of infrared materials (ZnS, Al_2O_3 and $MgAl_2O_4$) that have been widely used in extreme environments and under severe loads, such as aerospace applications[7]. Recently, progress of the composite ceramic as a competitive candidate in this area brings new driving power.

Among all nano-composite ceramics, the Y_2O_3-MgO nano-composite ceramics are presentative infrared transparent ceramic, since the Y_2O_3-MgO nano-composite ceramics process outstanding thermal and mechanical properties for extreme environments[8-10]. The most commonly approach to sintering Y_2O_3-MgO nano-composite ceramics is the spark plasma sintering(SPS). SPS regarded as a rapid solidification sintering method is an especially efficient technique, through which the sintering time can be massively decreased owing to the rapid heating rate at a speed higher than 100 ℃/min compared with conventional sintering methods. For the pressureless sintering, the higher sintering temperature and the longer sintering time lead to dramatically grain growth, particularly in the final period of the densification. For another, SPS enhances the driving force of sintering by dynamically activating plastic deformation and diffusion processes, which is efficacious to restrict the grain growth under a lower sintering temperature and high intensity of pressure. In 2010, Jiang et al.[11] prepared Y_2O_3-MgO nano-composite ceramics with the grain size less than 100 nm by SPS sintering under a load of 80 MPa. Liu et al.[12] used SPS to sinter the powders after ultrasonic horn treatment to prepare the Y_2O_3-MgO nano-composite ceramics at 50 MPa. Huang et al.[13] prepared the Y_2O_3-MgO nano-composite ceramics with a grain size of 100 – 200 nm through SPS sintering with 100 MPa. Then, Xu et al.[14] prepared the Y_2O_3-MgO nano-composite ceramics with a grain size of 100 – 300 nm through SPS sintering under 50 MPa, which got the nano-powder through the esterification sol-gel route. Recently, Safronova et al.[15] explored the influence of temperature on the Y_2O_3-MgO nano-composite ceramics during SPS sintering. At the same time, Liu et al.[16] and Ma et al.[17] independently explored the influence of pressure and LiF sintering aid on grain growth of Y_2O_3-MgO ceramics.

For obtaining Y_2O_3-MgO nano-composite ceramics, the preparation method of Y_2O_3-MgO nano-powders is as important as the sintering process. The high sinterability and homogeneity of nano-powders are critical parameters for obtaining the smaller grain-sized composite ceramics with high transmittance in the infrared band. So far, the preparation methods of Y_2O_3-MgO nano-powders mainly including spray pyrolysis[11,18], sol-gel method[19-24], glycine-nitrate process[25-26] and sol-gel combustion method[27-30] were systematically studied. The above methods can produce nano-size Y_2O_3 and MgO powders. However, these powder preparation methods still exist some problems, such as relatively expensive raw materials, long powder preparation cycles,

relatively high equipment requirements and uncontrollable reaction processes. Urea precipitation is a kind of powder preparation method with simple operation, short reaction period, uniform system, and controllable precipitation process[31-32]. Urea is an easily available and relatively environmentally friendly precipitant. In the reaction process, urea decomposes slowly until the solution rises to $80 - 90$ ℃, and a large amount of urea begins to decompose, producing OH^- and CO_3^{2-}, and forming a great amount of precipitation within a short period[33-34]. However, the precipitation variables of dual cations are complex and difficult to control, so the introduction of nano-particles as cores can induce the precipitation of precursors onto the surface of nano-particles through heterogeneous phase formation to form a core-shell structure, thus simplifying the variables in the process of preparing nano-composite powders by urea precipitation[35-38]. The mechanism of the self-assembled core-shell precursors can be divided into two stages. First, as urea hydrolysis began, the precipitant groups of OH^-, CO_3^{2-} and HCO_3^- were formed and modified the surface of the nano-particle. The Y-compound was pre-coated on the surface of nano-particles, driven by electrostatic attraction. Secondly, the assembly of the tiny Y-compound particles is formed in the burst nucleation process onto nano-particle surface, mainly driven by its high surface energy[39-42]. Meanwhile, the size of the powder is bound by the core-shell structure, so that the grains do not grow excessively during the sintering process.

In present work, the homogenous Y_2O_3-MgO core-shell structure nano-powders were prepared through urea precipitation approach. In order to obtain high sinterability powders, the calcination temperature, powder morphology and size of Y_2O_3-MgO core-shell structure nano-powders were studied compared with that of single-phase Y_2O_3. Y_2O_3-MgO composite nano-ceramics were sintered by SPS using core-shell powders as the beginning powders. This core-shell nano-powders preparation method and SPS procedure are simple and inexpensive, which provide a novel way to fabricate Y_2O_3-MgO composite nano-ceramics.

2   Experimental and Characterizations

Y_2O_3-MgO core-shell structure nano-powders were prepared by urea precipitation. The raw materials were Y_2O_3(5N), nitric acid(AR), urea(99%), and MgO(99.9%, 50 nm). Firstly, 0.015 mol $Y(NO_3)_3$ solution was prepared by dissolving 0.007 5 mol Y_2O_3 in a certain number of HNO_3. Next, $Y(NO_3)_3$ solution was added together with 0.5 mol urea into a three-necked flask of 2 000 mL. Then, MgO was weighted with a volume ratio of 1∶1 to Y_2O_3 into the container through stirring and dispersing sufficiently. After that, MgO was transferred to the solution in the three-necked flask. Currently, there were about 1 300 mL of solution in the three-necked flask. Finally, the three-necked flask was placed in a heating mantle to heat the solution temperature from room temperature to (85 ± 1) ℃ in about 40 min. At the same time, an electric stirrer was used to stir at a rate of 500 r/min. When the solution was obviously turbid, the reaction was maintained in this state for 2 h. After two hours, the resulting suspension was obtained by suction filtration, and then the suspension was placed in an oven and dried at 80 ℃ for 24 h. The dried precursors were put into the muff furnace and calcined at the selected temperature for 1 h, after which 0.25% LiF(99%) was added and the powders were ground, and then screened with a 140-mesh sieve.

Transparent Y_2O_3 ceramics powders were also prepared by urea precipitation method, and then ground and screened with 140 mesh, and then compressed into φ10 discs by a powder tablet machine. The ceramic tablets were compacted at 200 MPa using a cold isostatic press. The sintering method was vacuum sintering, the temperature was 1 750 ℃, and the holding time was 4 h.

The powders obtained above were sintered into ceramics through SPS (LABOX-1575, SinterL and Inc., Japan). The powder samples loaded into the graphite mold were heated from room temperature to a pre-set temperature(1 200 ℃) at the heating rate of 100 ℃/min under vacuum(10 Pa) and the dwell

time was 8 min with the pressure of 50 MPa. The sintered Y_2O_3-MgO composite nano-ceramics were annealed in the air at 1 000 ℃ for 15 h to eliminate oxygen vacancies, carbon and residual stress. When measuring infrared transmittance, the sample is polished on both sides to a thickness of ~0.9 mm.

XRD patterns were measured by a Bruker D8 X-ray diffractometer with Cu Kα radiation (λ = 0.154 056 nm) at 40 kV and 40 mA. Thermal analysis of the precursors was measured by thermogravimetric/differential scanning calorimetry (TG/DSC, STA 449F3, NETZSCH, Germany) at a heating rate of 10 K/min in air. A thermal field emission scanning electron microscope(TFE-SEM, Thermo Scientific Verios G4 UC) was used to observe the microscopic morphology of the powders. The particle size distributions of the powders were measured by Laser particle size analyzer (HELOS-OASIS, Sympatec GmbH, Germany). The grain and grain boundary morphology of the ceramic were measured by a field emission scanning electron microscope (FE-SEM, Hitachi S4800, Japan). The transmittance in the wavelength range of $\lambda = 0.25 - 2.5$ μm was conducted by using a spectrometer (Lambda 950, Perkin Elmer Co., USA). Fourier transform infrared spectroscopy(NICOLET 6700, Thermo Co, USA) was used to measure the transmittance of the mirror polished samples at a range of $2.5 - 10$ μm. An image analysis microhardness tester(HV-1000/S, SIOMM, Shanghai) was used to carry out a 10 s, 100 N load test to obtain the Vickers hardness result.

3　Results and Discussion

Fig. 1 shows TG/DSC curves of the Y_2O_3-MgO core-shell structure nano-powder precursors. In the process from room temperature to 870 ℃, the total mass loss is 34.1%, which can be divided into four periods. The first period is from room temperature to 185.7 ℃, with a mass loss of 8.0%, and an endothermic peak at 137.5 ℃ is due to the evaporation of absorbed water and the release of bound water. The mass loss in the second period is 13.9%, which occurs in the temperature range between 185.7 and 422.6 ℃. The exothermic peaks at 226 ℃ and 286

℃ are mainly caused by the decomposition and oxidation of NO_3^- ions. The third period is 422.6 ℃ to 598.8 ℃, and its mass loss is 8.4%. Among them, there is an endothermic peak at 492.8 ℃ and 568 ℃, which is caused by the decomposition of hydroxides and carbonates. The 3.8% mass loss occurs in the last period, and there is an exothermic peak at 653.3 ℃, which is related to the crystallization of the Y_2O_3 crystals. The results of TG-DSC curves indicate Y_2O_3-MgO core-shell structure nano-powders can be obtained at 750 ℃.
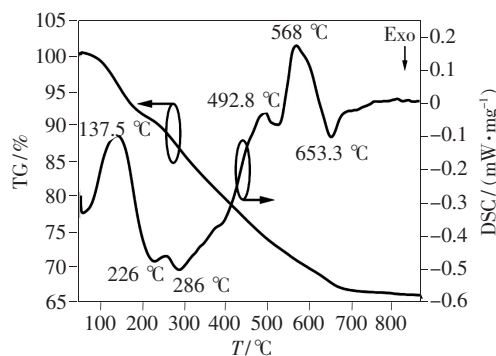

Fig. 1　TG-DSC curves of the Y_2O_3-MgO core-shell structure nano-powder precursors

Fig. 2 shows XRD patterns of MgO nano-powders, Y_2O_3 nano-powder precursors, Y_2O_3-MgO core-shell structure nano-powder precursors and Y_2O_3-MgO core-shell structure nano-powders calcined at different temperatures. Compared with Y_2O_3 nano-powder precursors, Y_2O_3-MgO core-shell structure nano-powder precursors appear weaker MgO peaks. The other peaks may be caused by the formation of the coating structure and some changes in the disordered structure of the outer layer. According to thermal analysis, the powders have reached its crystallization temperature at 650 ℃. After reaching 750 ℃, the powders have been completely crystallized, and no obvious heat absorption and exotherm were observed, and the quality almost no longer changes. As a result, 750 ℃ is the optimum calcination temperature for the powders. The XRD of core-shell structure nano-powders calcined at 650, 750, 850 ℃ are consistent with that of Y_2O_3 and MgO, and there is no obvious change between them, except that the peak shape gradually becomes sharp with the increase of temperature, indicating that

the powders have basically formed phase at 650 ℃. Therefore, the calcined temperature of Y_2O_3-MgO core-shell structure nano-powder precursors is higher about 100 ℃ than precursor crystallization temperature in order to remove possible traces of carbon- and nitrogen-containing compounds.
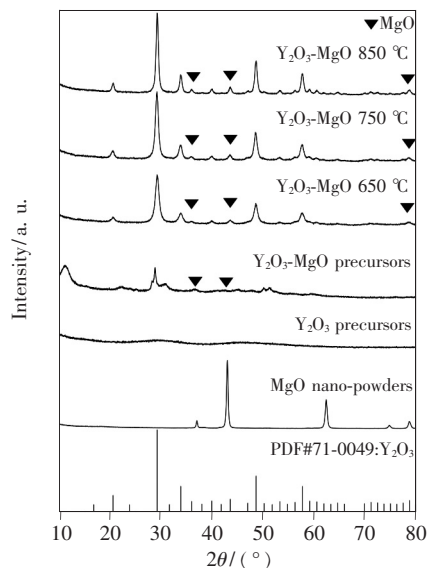

Fig. 2　XRD patterns of MgO nano-powders, Y_2O_3 nano-powder precursors, Y_2O_3-MgO core-shell structure nano-powder precursors and Y_2O_3-MgO core-shell structure nano-powders calcined at different temperatures.

Fig. 3 shows the micromorphology of MgO nano-powders, Y_2O_3 powders, Y_2O_3-MgO core-shell structure nano-powder precursors and Y_2O_3-MgO core-shell structure nano-powders. The powder size of MgO nano-powders in Fig. 3(a) is about 50 nm, and the powder morphology are relatively uniform. Fig. 3(b) shows the prepared Y_2O_3 powders by the urea precipitation method. The size of Y_2O_3 powders with good sphericity and good monodispersity is about 200 – 300 nm. The micrograph of Y_2O_3-MgO core-shell structure nano-powder precursors (Fig. 3(c)) is much more similar to that of MgO nano-powders due to the nucleation process starting on the surface of MgO nano-powders. As shown in Fig. 3(d), Y_2O_3-MgO core-shell structure nano-powders with soft agglomeration are composed of microcrystals. Y_2O_3-MgO core-shell structure nano-powders exhibit a clear interface between core and shell,

which indicates the MgO nano-powders as a core are successfully cladded with Y_2O_3 powders as a shell. The size distribution of all the powders is shown in Fig. 4. Compared with the SEM images, the four kinds of powders have different degrees of agglomeration. Fig. 4(a) shows the particle size distribution of MgO nano-powders is around 600 nm, which is quite different from the SEM image. This is due to the small size of MgO nano-powders and large specific surface area, which is easy to form large agglomerated particles. According to Fig. 4(b), the size of Y_2O_3 powders is mainly concentrated in 200 – 300 nm, which is more consistent with Fig. 3(b) image. Therefore, the larger particles are ascribed to slightly agglomerating of Y_2O_3 powders. Fig. 4(c) shows that the particle size distribution of Y_2O_3-MgO core-shell structure nano-powder precursors is mainly 100 – 300 nm. Since the precursors have not undergone crystallization after calcination, the particles have not grown. From Fig. 4(d), the agglomeration of Y_2O_3-MgO core-shell structure nano-powders nearly disappear with uniform size distribution at about 250 nm. After calcined at low temperature, the inorganic acid ions are decomposed and core-shell structure powders did not happen growing up. Fig. 5 shows the EDS mapping images of Y_2O_3-MgO core-shell structure nano-powders calcined at 750 ℃. As represented in Fig. 5, Y, Mg and O elements are evenly distributed throughout Y_2O_3-MgO core-shell

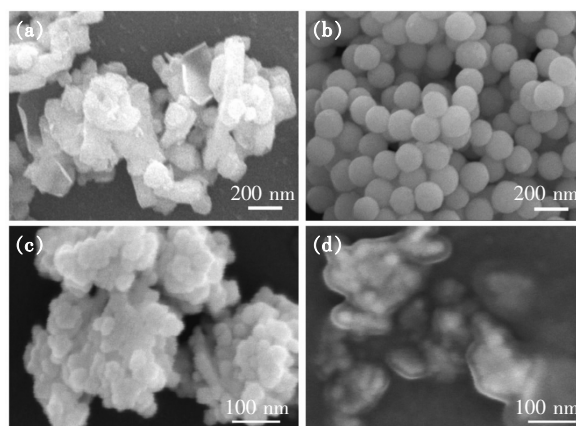Fig. 3　SEM images of MgO nano-powders(a), Y_2O_3 powders(b), Y_2O_3-MgO core-shell structure nano-powder precursors(c), Y_2O_3-MgO core-shell structure nano-powders(d).
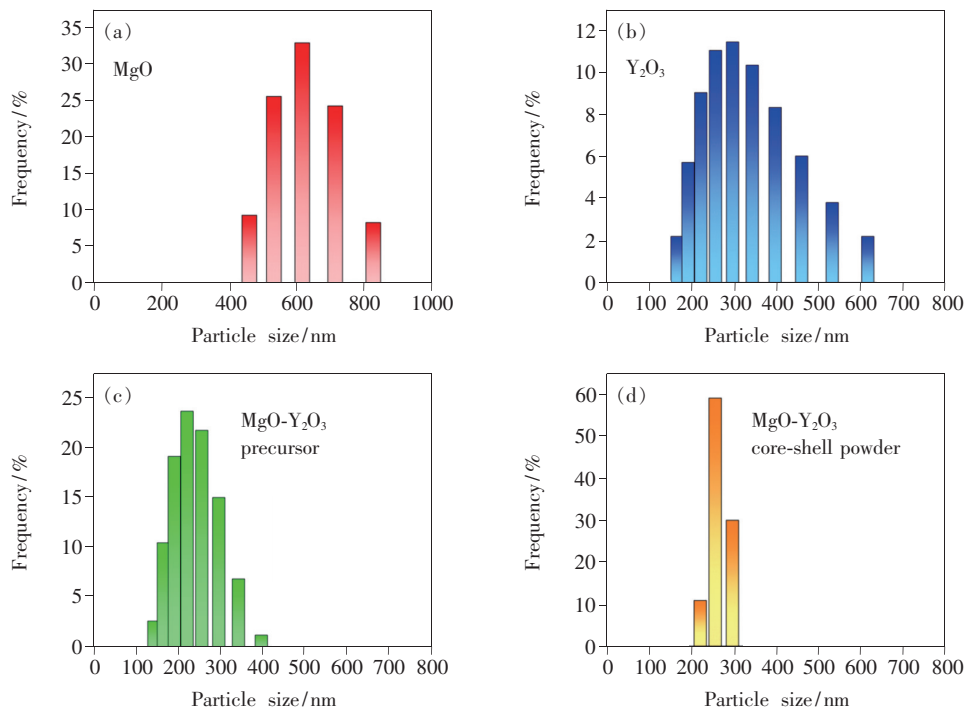
Fig. 4　Particle size distributions of MgO nano-powders(a), Y$_2$O$_3$ powders(b), Y$_2$O$_3$-MgO core-shell structure nano-powder precursors(c), Y$_2$O$_3$-MgO core-shell structure nano-powders(d).
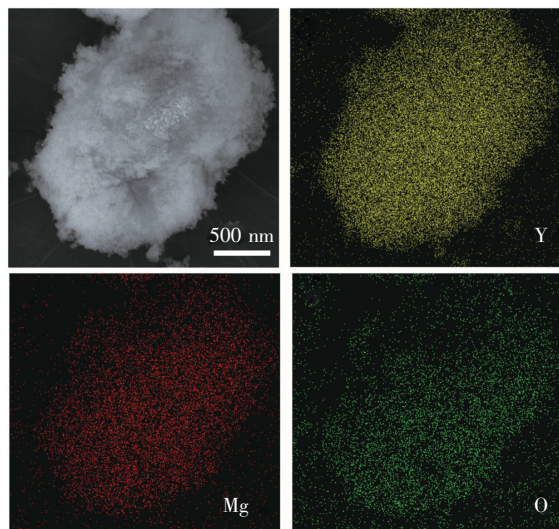

Fig. 5　EDS mapping images of Y$_2$O$_3$-MgO core-shell structure nano-powders calcined at 750 ℃

structure nano-powders. However, the content distribution of Y is denser than that of Mg due to Y distributing on the outer surface of core-shell structure.

Fig. 6 shows the micro-morphology of Y$_2$O$_3$ ceramics and Y$_2$O$_3$-MgO composite nano-ceramics, and the EDS mapping images of Y$_2$O$_3$-MgO composite nano-ceramics. From Fig. 6 (a) and (b), the average grain size of the Y$_2$O$_3$ ceramics is about 100 μm, while the average grain size of the Y$_2$O$_3$-MgO

composite nano-ceramics is about 360 nm. It can be seen from the image that Y$_2$O$_3$ ceramics show larger grains and irregular grain growth, while the grains of Y$_2$O$_3$-MgO composite nano-ceramics are smaller and the grain growth is more uniform. Following BSE images and EDS mapping images, in Fig. 6 (d), the white phase and black phase are respectively Y$_2$O$_3$ and MgO. At the same time, the grain size of MgO is generally smaller than that of Y$_2$O$_3$, and the larger MgO grains may be caused by the incomplete coating structure. And from the Fig. 6 (d), obviously, it can be seen that the black phase is surrounded by the white phase, that is, MgO is surrounded by Y$_2$O$_3$, which corresponds to the prepared core-shell structure nano-powders, thus confirming the construction of the core-shell structure. The core-shell structure nano-powders are beneficial to a more even distribution of the two grains, which is conducive to inhibiting growth of ceramic grains in a smaller scale. It indicates that the core-shell structure nano-powders has a certain binding effect on the grain growth during sintering, making the grains unable to grow at will.

Fig. 7 shows IR transmittance spectra of Y$_2$O$_3$ ceramics and Y$_2$O$_3$-MgO composite nano-ceramics.
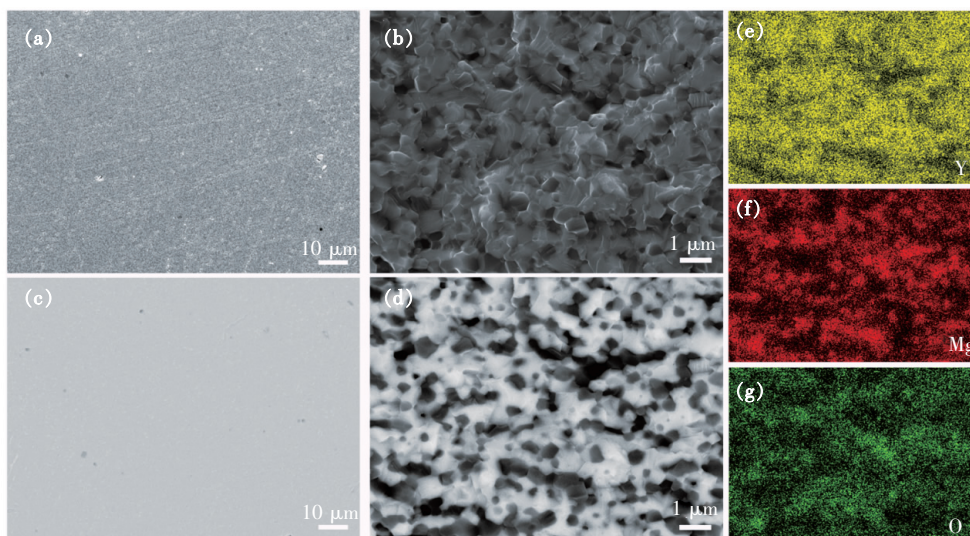
Fig. 6   SEM images of Y$_2$O$_3$ ceramics(a) and Y$_2$O$_3$-MgO composite nano-ceramics(b). BSE images of Y$_2$O$_3$ ceramics(c) and Y$_2$O$_3$-MgO composite nano-ceramics(d). (e) – (g)EDS mapping images of (b).
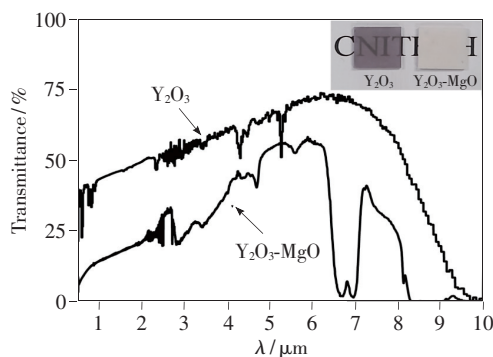

Fig. 7   IR transmittance spectra of Y$_2$O$_3$ ceramics and Y$_2$O$_3$-MgO composite nano-ceramics with the thickness of 0.9 mm. Inset：the photo of synthesized Y$_2$O$_3$ ceramics(left) and Y$_2$O$_3$-MgO composite nano-ceramics(right).

The transmittance of Y$_2$O$_3$ ceramics is higher than that of Y$_2$O$_3$-MgO composite nano-ceramics and reaches nearly 75% at about 6.5 μm, and the cut-off wavelength is about 10 μm. From the image, the Y$_2$O$_3$ ceramic is translucent, while the Y$_2$O$_3$-MgO composite nano-ceramic is completely opaque white at visual light range, which is more consistent with the results of the transmittance spectra. The transmittance of Y$_2$O$_3$ ceramics fluctuates at 3 μm, which should be due to the influence of residual water in the pores(the characteristic absorption peak of —OH is 2.94 – 3.12 μm), and the absorption peak of 4.3 μm coincides with the characteristic absorption peak of CO$_2$ (the characteristic absorption peak of

CO$_2$ is 4.26 μm). These two absorption peaks may be trapped in the pores and not removed during the sintering process, so it makes the characteristic absorption peaks appear when measuring the infrared transmittance. The low transmittance of Y$_2$O$_3$-MgO composite nano-ceramics may be due to the improper ratio of Y$_2$O$_3$ to MgO when preparing powders, low density of the ceramics, improper sintering temperature program and other factors that affect the performance, which need to be further studied and improved. From the infrared transmittance of Y$_2$O$_3$-MgO composite nano-ceramics, the transmittance at wavelength of 6 μm is the highest, reaching 57%, and the cut-off wavelength is about 8.3 μm. Similar to Y$_2$O$_3$ ceramics, the transmittance of composite nano-ceramics has absorption peaks at 3 μm and 4.3 μm, that is, water and CO$_2$ exist in pores. The difference is that the composite nano-ceramics also have strong absorption peaks around 4.7 μm and 6.8 μm. The absorption peak at 4.7 μm matches the characteristic absorption peak of CO(the characteristic absorption peak of CO is 4.65 μm), while the absorption peak at 6.8 μm. The peak is more consistent with the characteristic absorption peak of CO$_3^{2-}$(the characteristic absorption peak of CO$_3^{2-}$ is 6.54 – 7.58 μm). The generation of these impurities is due to the carburizing phenomenon that occurs during SPS sintering. Although LiF sintering aid is

added during sintering, the density of the ceramics is improved to a certain extent and some carbon is taken away, but the density is still not high enough to make the carburizing phenomenon disappear.

Fig. 8 shows the comparison of Vickers hardness of Y_2O_3 ceramics and Y_2O_3-MgO composite nano-ceramics. The Vickers hardness of Y_2O_3 ceramics is about 780 HV, and the Vickers hardness of Y_2O_3-MgO composite nano-ceramics is about 820 HV. Compared with Y_2O_3 ceramics, after adding MgO, its mechanical properties have indeed improved. However, its hardness is far from reaching the required level, so the powder preparation and sintering process still need to be improved.
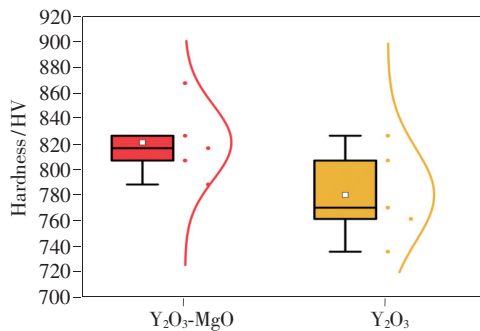

Fig. 8   Vickers hardness of Y_2O_3 ceramics and Y_2O_3-MgO composite nano-ceramics

4   Conclusion

Y_2O_3-MgO core-shell structure nano-powders with the particle size of about 250 nm were successfully prepared by urea precipitation method. Y_2O_3-MgO composite nano-ceramics with the average grain size of 360 nm are accomplished *via* SPS treatment. Grain size of Y_2O_3-MgO composite nano-ceramics is more uniform and smaller compared with Y_2O_3 ceramics, indicating that the core-shell structure has certain binding effect on the grain growth. This core-shell structure nano-powders preparation method offers a new approach to further control the grain size of nano-composite ceramics. However, the transmittance and Vickers hardness of Y_2O_3-MgO composite nano-ceramics are not good enough, so the powder preparation and sintering process still need to be explored. Together with the SPS treatment, the method accomplished in this work provides a novel way to fabricate Y_2O_3-MgO composite nano-ceramics.

Response Letter is available for this paper at: http:// cjl. lightpublishing. cn/thesisDetails#10. 37188/CJL. 20210095.

References:

[1] HARRIS D C. Durable 3 – 5 μm transmitting infrared window materials [J]. *Infrared Phys. Technol.*, 1998,39(4): 185-201.

[2] JAIN M,SKANDAN G,SINGHAL A,*et al*. Synthesis and processing of nanocrystalline powders for IR transparent windows [C]. *Proceedings of SPIE*, *Window and Dome Technologies and Materials IX*,*Orlando*,*Florida*,*United States*, 2005:217-226.

[3] 张松涛,王樱蕙,张洪杰. 稀土发光材料在近红外二区成像中的应用 [J]. 发光学报, 2020,41(12):1460-1478.
ZHANG S T,WANG Y H,ZHANG H J. Lanthanide-doped fluorescence probes for NIR-Ⅱ fluorescence imaging [J]. *Chin. J. Lumin.*, 2020,41(12):1460-1478. (in Chinese)

[4] 刘钟馨,宋宏伟. 银纳米链状材料的制备及近红外吸收性质 [J]. 发光学报, 2008,29(6):1067-1070.
LIU Z X,SONG H W. Synthesis of Ag nanochains and near-infrared absorption property [J]. *Chin. J. Lumin.*, 2008,29 (6):1067-1070. (in Chinese)

[5] 刘庆生,常晴,李江霖,等. LaCoO₃ 及 Ca-Fe 共掺陶瓷材料的制备及红外发射率研究 [J]. 发光学报, 2018,39(8): 1066-1074.
LIU Q S,CHANG Q,LI J L,*et al*. Preparations and infrared emissive properties of LaCoO₃ and Ca-Fe Co-doped ceramics [J]. *Chin. J. Lumin.*, 2018,39(8):1066-1074. (in Chinese)

[6] KRELL A,KLIMKE J,HUTZLER T. Transparent compact ceramics:inherent physical issues [J]. *Opt. Mater.*, 2009,31 (8):1144-1150.

[7] WANG S F,ZHANG J,LUO D W,*et al*. Transparent ceramics:processing, materials and applications [J]. *Prog. Solid*

State Chem. , 2013,41(1-2):20-54.

[8] XIE J X,MAO X J,ZHU Q Q,*et al.* Influence of synthesis conditions on the properties of Y_2O_3-MgO nanopowders and sintered nanocomposites [J]. *J. Eur. Ceram. Soc.* , 2017,37(13): 4095-4101.

[9] GHORBANI S,LOGHMAN-ESTARKI M R,RAZAVI R S,*et al.* A new method for the fabrication of MgO-Y_2O_3 composite nanopowder at low temperature based on bioorganic material [J]. *Ceram. Int.* , 2018,44(3):2814-2821.

[10] JUNG W K,MA H J,KIM H N,*et al.* Transparent ceramics for visible/IR windows：processing,materials and characterization [J]. *Korean J. Mater. Res.* , 2018,28(10):551-563.

[11] XIE J X,MAO X J,LI X K,*et al.* Influence of moisture absorption on the synthesis and properties of Y_2O_3-MgO nanocomposites [J]. *Ceram. Int.* , 2017,43(1):40-44.

[12] WILLINGHAM C B,WAHL J M,HOGAN P K,*et al.* Densification of nano-yttria powders for IR window applications [C]. *Proceedings of SPIE,Window and Dome Technologies Ⅷ,Orlando,Florida,United States*, 2003:179-188.

[13] HARRIS D C,CAMBREA L R,JOHNSON L F,*et al.* Properties of an infrared-transparent MgO：Y_2O_3 nanocomposite [J]. *J. Am. Ceram. Soc.* , 2013,96(12):3828-3835.

[14] JIANG D T,MUKHERJEE A K. Spark plasma sintering of an infrared-transparent Y_2O_3-MgO nanocomposite [J]. *J. Am. Ceram. Soc.* , 2010,93(3):769-773.

[15] LIU J,YAO W L,KEAR B,*et al.* Microstructure and IR transmittance of yttria-magnesia (50:50 vol.%) nano-composites consolidated from agglomerated and ultrasonic horn treated nano-powders [J]. *Mater. Sci. Eng.* B, 2010,171(1-3): 149-154.

[16] HUANG L,YAO W L,LIU J,*et al.* Spark plasma sintering and mechanical behavior of magnesia-yttria(50: 50 vol.%) nanocomposites [J]. *Scr. Mater.* , 2014,75:18-21.

[17] XU S Q,LI J,KOU H M,*et al.* Spark plasma sintering of Y_2O_3-MgO composite nanopowder synthesized by the esterification sol-gel route [J]. *Ceram. Int.* , 2015,41(2):3312-3317.

[18] SAFRONOVA N A,KRYZHANOVSKA O S,DOBROTVORSKA M V,*et al.* Influence of sintering temperature on structural and optical properties of Y_2O_3-MgO composite SPS ceramics [J]. *Ceram. Int.* , 2020,46(5):6537-6543.

[19] LIU L H,MORITA K,SUZUKI T S,*et al.* Evolution of microstructure,mechanical,and optical properties of Y_2O_3-MgO nanocomposites fabricated by high pressure spark plasma sintering [J]. *J. Eur. Ceram. Soc.* , 2020, 40 (13): 4547-4555.

[20] MA H J,KONG J H,KIM D K. Insight into the scavenger effect of LiF on extinction of a carboxylate group for mid-infrared transparent Y_2O_3-MgO nanocomposite [J]. *Scr. Mater.* , 2020,187:37-42.

[21] KEAR B H,SADANGI R,SHUKLA V,*et al.* Submicron-grained transparent yttria composites [C]. *Proceedings of SPIE, Window and Dome Technologies and Materials IX, Orlando,Florida,United States*, 2005:227-233.

[22] LIU L H,MORITA K,SUZUKI T S,*et al.* Synthesis of highly-infrared transparent Y_2O_3-MgO nanocomposites by colloidal technique and SPS [J]. *Ceram. Int.* , 2020,46(9):13669-13676.

[23] MUOTO C K,JORDAN E H,GELL M,*et al.* Phase homogeneity in Y_2O_3-MgO nanocomposites synthesized by thermal decomposition of nitrate precursors with ammonium acetate additions [J]. *J. Am. Ceram. Soc.* , 2011, 94 (12): 4207-4217.

[24] CHEN C H,GAROFANO J K M,MUOTO C K,*et al.* A foaming esterification sol-gel route for the synthesis of magnesia-yttria nanocomposites [J]. *J. Am. Ceram. Soc.* , 2011,94(2):367-371.

[25] IYER A,GAROFANO J K M,REUTENAUR J,*et al.* A sucrose-mediated Sol-Gel technique for the synthesis of MgO-Y_2O_3 nanocomposites [J]. *J. Am. Ceram. Soc.* , 2013,96(2):346-350.

[26] GHORBANI S,RAZAVI R S,LOGHMAN-ESTARKI M R,*et al.* Synthesis of MgO-Y_2O_3 composite nanopowder with a high specific surface area by the Pechini method [J]. *Ceram. Int.* , 2017,43(1):345-354.

[27] VAEZ S H,LOGHMAN-ESTARKI M R,RAZAVI R S,*et al.* Novel nano-dimensional cubic-spherical morphology for $(Y_2O_3)_{0.5}$-$(MgO)_{0.5}$ nanocomposite:synthesis and optical properties [J]. *Ceram. Int.* , 2018,44(17):21099-21106.

[28] MA H J,JUNG W K,PARK Y,*et al.* A novel approach of an infrared transparent Er:Y_2O_3-MgO nanocomposite for eye-safe laser ceramics [J]. *J. Mater. Chem.* C, 2018,6(41):11096-11103.

[29] MA H J,JUNG W K,BAEK C,*et al.* Influence of microstructure control on optical and mechanical properties of infrared transparent Y_2O_3-MgO nanocomposite [J]. *J. Eur. Ceram. Soc.* , 2017,37(15):4902-4911.

［30］ WANG J W,CHEN D Y,JORDAN E H,*et al*. Infrared-transparent Y_2O_3-MgO nanocomposites using sol-gel combustion synthesized powder ［J］. *J. Am. Ceram. Soc.*，2010,93(11):3535-3538.

［31］ PERMIN D A,BOLDIN M S,BELYAEV A V,*et al*. IR-transparent MgO-Y_2O_3 ceramics by self-propagating high-temperature synthesis and spark plasma sintering ［J］. *Ceram. Int.*，2020,46(10):15786-15792.

［32］ XU S Q,LI J,LI C Y,*et al*. Infrared-transparent Y_2O_3-MgO nanocomposites fabricated by the glucose sol-gel combustion and hot-pressing technique ［J］. *J. Am. Ceram. Soc.*，2015,98(9):2796-2802.

［33］ XU S Q,LI J,LI C Y,*et al*. Hot pressing of infrared-transparent Y_2O_3-MgO nanocomposites using sol-gel combustion synthesized powders ［J］. *J. Am. Ceram. Soc.*，2015,98(3):1019-1026.

［34］ YANG Y M,ZHAO X F,ZHU Y,*et al*. Transformation mechanism of magnesium and aluminum precursor solution into crystallites of layered double hydroxide ［J］. *Chem. Mater.*，2012,24(1):81-87.

［35］ JUNG W K,MA H J,JUNG S W,*et al*. Effects of calcination atmosphere on monodispersed spherical particles for highly optical transparent yttria ceramics ［J］. *J. Am. Ceram. Soc.*，2017,100(5):1876-1884.

［36］ FUJITA Y,TAYLOR J L,GRESHAM T L T,*et al*. Stimulation of microbial urea hydrolysis in groundwater to enhance calcite precipitation ［J］. *Environ. Sci. Technol.*，2008,42(8):3025-3032.

［37］ ITO T,INUMARU K,MISONO M. Epitaxially self-assembled aggregates of polyoxotungstate nanocrystallites,$(NH_4)_3PW_{12}O_{40}$: synthesis by homogeneous precipitation using decomposition of urea ［J］. *Chem. Mater.*，2001,13(3):824-831.

［38］ CHANG H Y,CHENG S Y,SHEU C I. Controlling interface characteristics by adjusting core-shell structure ［J］. *Acta Mater.*，2004,52(18):5389-5396.

［39］ SANG Y H,QIN H M,LIU H,*et al*. Partial wet route for YAG powders synthesis leading to transparent ceramic:a core-shell solid-state reaction process ［J］. *J. Eur. Ceram. Soc.*，2013,33(13-14):2617-2623.

［40］ KAFILI G,LOGHMAN-ESTARKI M R,MILANI M,*et al*. The effects of TEOS on the microstructure and phase evolutions of YAG phase by formation of alumina/yttria core-shell structures ［J］. *J. Am. Ceram. Soc.*，2017,100(9):4305-4316.

［41］ CHEN Y X,ZENG X Z,ZHU J T,*et al*. High performance and enhanced durability of thermochromic films using VO_2@ZnO core-shell nanoparticles ［J］. *ACS Appl. Mater. Interfaces*，2017,9(33):27784-27791.

［42］ DING H,QIN H M,FENG S W,*et al*. Full spectrum core-shell phosphors under ultraviolet excitation ［J］. *Chem. Commun.*，2019, 55(81):12188-12191.

江宏涛(1995 -)，男，浙江平湖人，硕士研究生，2018 年于南京工业大学获得学士学位，主要从事红外窗口材料的制备与研究。

E-mail：jianghongtao@ nimte. ac. cn

陈红兵(1964 -)，男，陕西汉阴人，博士，教授，1997 年于中国科学院上海光学精密机械研究所获得博士学位，主要从事新型闪烁材料、高性能弛豫铁电材料、非线性光学材料、闪烁陶瓷材料的单晶生长、性能表征与器件应用的研究。

E-mail：chenhongbing@ nbu. edu. cn

冯少尉(1990 -)，男，山东泰安人，博士研究生，2018 年于上海大学获得硕士学位，主要从事透明光功能陶瓷的研究。

E-mail：swfeng@ ipe. ac. cn